

## Phase transition induced micromechanical actuation in VO<sub>2</sub> coated cantilever

Bharathi Rajeswaran, L. R. Viannie, K. Rajanna, G. R. Jayanth, and A. M. Umarji

Citation: *Journal of Applied Physics* **124**, 074502 (2018); doi: 10.1063/1.5031856

View online: <https://doi.org/10.1063/1.5031856>

View Table of Contents: <http://aip.scitation.org/toc/jap/124/7>

Published by the [American Institute of Physics](#)

---

### Articles you may be interested in

[Independent indistinguishable quantum light sources on a reconfigurable photonic integrated circuit](#)  
*Applied Physics Letters* **112**, 211104 (2018); 10.1063/1.5028339

[Power dissipation in the mixed metal-insulator state of self-heated VO<sub>2</sub> single crystals and the effect of sliding domains](#)  
*Applied Physics Letters* **112**, 231905 (2018); 10.1063/1.5029519

[Structured ultrasound microscopy](#)  
*Applied Physics Letters* **112**, 251901 (2018); 10.1063/1.5026863

[Magnetotransport properties of perovskite EuNbO<sub>3</sub> single-crystalline thin films](#)  
*Applied Physics Letters* **113**, 032401 (2018); 10.1063/1.5034037

[Growth of ordered arrays of vertical free-standing VO<sub>2</sub> nanowires on nanoimprinted Si](#)  
*Applied Physics Letters* **113**, 043101 (2018); 10.1063/1.5031075

[The Hartman effect in Weyl semimetals](#)  
*Journal of Applied Physics* **124**, 064301 (2018); 10.1063/1.5035304

---

**AIP** | Journal of Applied Physics SPECIAL TOPICS



## Phase transition induced micromechanical actuation in VO<sub>2</sub> coated cantilever

Bharathi Rajeswaran,<sup>1,a),b)</sup> L. R. Viannie,<sup>2,a),b)</sup> K. Rajanna,<sup>2</sup> G. R. Jayanth,<sup>2</sup> and A. M. Umarji<sup>1</sup>

<sup>1</sup>Materials Research Centre, Indian Institute of Science, Bangalore 560012, India

<sup>2</sup>Department of Instrumentation and Applied Physics, Indian Institute of Science, Bangalore 560012, India

(Received 1 April 2018; accepted 22 July 2018; published online 20 August 2018)

Structural phase transition assisted micromechanical actuation of a vanadium dioxide (VO<sub>2</sub>) coated silicon microcantilever is presented. A 300 nm polycrystalline VO<sub>2</sub> film was deposited over the silicon surface at 520 °C using metal organic chemical vapor deposition. The formation of the M1 monoclinic phase of the as-deposited VO<sub>2</sub> film was confirmed by X-ray diffraction studies and further verified by temperature variable Raman spectroscopy. The heated VO<sub>2</sub> film exhibits semiconductor-to-metal transition at 74 °C, which produces a change in the electrical resistance almost of three orders in magnitude. Consequently, the VO<sub>2</sub> film undergoes structural phase transition from the monoclinic phase (011)<sub>M1</sub> to a tetragonal phase (110)<sub>R</sub>. This generates a compressive stress within the VO<sub>2</sub> film resulting in large, reversible cantilever deflection. This deflection was measured with a non-contact 3D optical profilometer, which does not require any vacuum conditions. Upon heating, the VO<sub>2</sub> coated silicon cantilever produced a large reversible tip deflection of 14 μm at 50 °C. Several heating and cooling cycles indicate steep changes in the cantilever tip deflection with negligible hysteresis. In addition, the effect of thermal stress induced cantilever deflection was estimated to be as small as 6.4%, and hence can be ignored. These results were found to be repeatable within controlled experimental conditions. *Published by AIP Publishing.*

<https://doi.org/10.1063/1.5031856>

### I. INTRODUCTION

Micro-electro-mechanical-system (MEMS) based microcantilevers are extensively used in RF switches,<sup>1</sup> micromanipulators,<sup>2-4</sup> micro-valves<sup>5</sup> and resonators.<sup>6</sup> These microcantilever structures are usually driven by electrostatic, piezoelectric, magnetic and thermal actuation mechanisms. Based on specific design requirements such as actuation force, displacement, power consumption, operating frequency, and temperature, appropriate actuation mechanisms may be adopted.<sup>6</sup> Fast response and high frequency operation may be achieved using electrostatic and piezoelectric actuators, while their deformations are much smaller.<sup>7-10</sup> Magnetically driven microactuators generate higher mechanical deformation and possess high operating frequencies. However, monolithic integration and miniaturization are much complex for magnetic actuators. Thermal actuators, on the other hand, produce large mechanical deformation but they too pose issues of elevated operating temperatures and higher power consumption, thereby posing problems for utilizing them under normal conditions.<sup>11,12</sup> In recent times, microcantilevers coated with vanadium dioxide (VO<sub>2</sub>) thin films have been employed for high speed, large reversible actuation and they are known to produce high strain energy densities as they show first order transition.<sup>13</sup> VO<sub>2</sub> is a strongly correlated oxide material which shows an accessible phase transition close to room temperature (~68 °C). This phase transition is often accompanied by a change in electrical

conductance,<sup>14</sup> optical transmittance,<sup>15</sup> and mechanical deformation.<sup>16,17</sup> Large distortion along the *c<sub>R</sub>*-axis of the unit cell is triggered by external stimuli such as temperature, radiation, and electrical potential resulting in the transition from the semiconducting monoclinic phase (M1, T < 68 °C) to a metallic rutile phase (R, T > 68 °C).<sup>18</sup> This semiconductor to metal transition (SMT) observed at 68 °C in VO<sub>2</sub> thin films produces an abrupt change in the resistivity of several orders of magnitude. Furthermore, SMT induces a mechanical deflection that is several magnitudes higher than conventional thermal actuators.<sup>14</sup> For this reason, VO<sub>2</sub> thin film coated MEMSs are often used as a thermomechanical switch due to its large actuation range and high speed actuation.<sup>17,19</sup>

The processing and deposition of VO<sub>2</sub> thin films significantly affect MEMS actuator's performance. Hence, process control is crucial in this type of study. Several reports indicate physical vapor deposition (PVD) based deposition techniques to produce high quality VO<sub>2</sub> thin films.<sup>20</sup> Although the films thus produced have desirable qualities like preferred crystallite orientation, controlled thicknesses, etc., other thin film techniques need to be studied. The crystallographic orientation of the as-deposited VO<sub>2</sub> film significantly affects the bending curvature of the microcantilever. Cao *et al.* report the fabrication of a single-crystal VO<sub>2</sub> microbeam by vapor transport method.<sup>17</sup> This report presents a higher bending curvature of the microbeam due to the single-crystal nature of the deposited VO<sub>2</sub> films. Also, Tselev *et al.* report the synthesis of single-crystalline VO<sub>2</sub> nanoplatelets on a Si/SiO<sub>2</sub> substrate by vapor transport method.<sup>21</sup> These structures produced a large change in the

<sup>a)</sup> Authors to whom correspondence should be addressed: rajeswaran.bharathi@gmail.com and roseviannie11@gmail.com

<sup>b)</sup> B. Rajeswaran and L. R. Viannie contributed equally to this work.

lattice parameters of VO<sub>2</sub> nanoplatelets upon electrical excitation ( $\sim 1\%$ ) owing to their single-crystalline nature. Cabrera *et al.* report the deposition of *c<sub>R</sub>*-axis oriented polycrystalline VO<sub>2</sub> films over amorphous SiO<sub>2</sub> using pulsed laser deposition (PLD) method.<sup>22</sup> Thermally induced structural phase transition in these VO<sub>2</sub> films produces contraction and subsequent bending of the bimorph cantilever structure. All these reports mention that single-crystalline VO<sub>2</sub> films produce superior mechanical actuation compared to polycrystalline films. The performance of the VO<sub>2</sub> coated microcantilever is majorly influenced by the quality of the deposited films and deposition parameters. The crystallinity of the underlying substrate material too enhances the quality of VO<sub>2</sub> films. Guo *et al.* illustrate the elastic properties and structural phase transition of VO<sub>2</sub> nanowires, which were studied using a push-to-pull MEMS structure and the corresponding phase transition was evaluated using X-ray microdiffraction with a transmission electron microscope (TEM).<sup>23</sup> This arrangement requires another MEMS and a special X-ray diffraction (XRD)-TEM arrangement to measure the deformations in VO<sub>2</sub> nanowires. Later, Cabrera *et al.* designed a microcantilever with an integrated heating element and two parallel electrodes. The current through the VO<sub>2</sub> film was measured to quantify phase change induced cantilever deflection.<sup>24</sup> This is an indirect method of deformation measurement and requires highly sensitive electronics to measure small cantilever deflections. Viswanath and Ramanathan illustrate direct *in-situ* monitoring of temperature induced structural phase transition in a VO<sub>2</sub> coated silicon cantilever using Fresnel contrast imaging with a transmission electron microscope (TEM).<sup>25</sup> The phase change induced cantilever deflection was measured by means of focus and defocus of the cantilever surface as seen via TEM images. Cabrera *et al.* report cantilever deflection measurement using laser deflection technique which involves the focusing of a collimated laser beam onto the surface VO<sub>2</sub> coated microcantilever and a reflected laser is made to incident on a photodetector. The relative positions of the laser spot on the photodetector with respect to the cantilever initial position determine the deflection of the cantilever.<sup>26</sup> Often, the VO<sub>2</sub> coated microcantilever is thermally excited using a Peltier heater or even laser assisted heating technique. This may cause an additional deflection in the VO<sub>2</sub> actuation and the laser spot must be focused to a very small dimension limited by the width of the cantilever. This type of deflection measurement requires a special optical beam deflection arrangement. Also, the focused laser spot could cause localized heating of the cantilever under study. Merced *et al.* used an optical microscope to image the thermomechanical deflection of the VO<sub>2</sub> microcantilever.<sup>27</sup> Although this method is simpler than earlier reports, it still suffers poor resolution.<sup>21–24</sup> On the other hand, the use of a transmission electron microscope for VO<sub>2</sub> actuation is of prime importance to study the basic material behavior about its transition temperature. Most of the deformation measurement techniques mentioned in earlier reports are expensive, indirect and requires highly trained personnel to carry out the measurements. Here, we present the phase transition induced static deflection measurement of a VO<sub>2</sub> coated silicon cantilever

using a non-contact 3D optical profilometer which overcomes the issue of heating using a laser light since the wavelength of light used in this technique is about 536 nm. Also, the measurement can be carried out under ambient conditions without any specific requirement of vacuum enclosure for a simple cantilever actuation study. In addition, the resolution of the measurement system was observed to be few hundred nanometers in range. Using 3D profiler technique, thermal actuation results revealed large, reversible mechanical deflection of the VO<sub>2</sub> coated silicon microcantilever with negligible hysteresis and good repeatability.

This paper presents thermomechanical actuation of a VO<sub>2</sub> coated silicon microcantilever due to phase transition induced cantilever deformation. Metal Organic Chemical Vapor Deposition (MOCVD) technique was used to deposit a continuous thin film of VO<sub>2</sub> over a single-crystal silicon microcantilever surface at 520 °C. The as-deposited thin film was characterized using XRD and Raman spectra. The fabricated actuator was heated from room temperature up to 100 °C and the corresponding cantilever deformation was measured using a non-contact 3D optical profilometer. The thermal actuation results revealed reversible mechanical deflection of the microcantilever with negligible hysteresis and good repeatability.

## II. EXPERIMENTAL PROCEDURES

Polycrystalline VO<sub>2</sub> thin films studied in this work were synthesized by a horizontal hot wall, low pressure, single step MOCVD technique. The schematic of MOCVD for the synthesis of vanadium oxides such as V<sub>2</sub>O<sub>5</sub>, V<sub>6</sub>O<sub>13</sub>, and VO<sub>2</sub> is reported elsewhere.<sup>28,29</sup> VO<sub>2</sub> films were deposited on commercially available silicon AFM probes which were procured from Nano And More, USA.

### A. Precursor preparation

MOCVD requires the use of a subliming precursor. The synthesis and characterization of this compound are detailed in the [supplementary material](#). A volatile metal organic precursor, vanadyl acetyl acetonate (VO(acac)<sub>2</sub>) was taken in an aluminum boat in the vaporizer. The deposition chamber was made of quartz which can be heated resistively to 1000 °C. High purity argon gas carried the precursor vapors to the reaction zone, whereas high purity oxygen gas acts like an oxidant (reactant gas) and was sent through a different line to the reaction zone. The cantilever substrates along with a few Si substrates were carefully placed in the holder inside the furnace and films were deposited at a temperature of 520 °C.

### B. Chemical vapor deposition of VO<sub>2</sub>

A schematic of the MOCVD setup is explained in [supplementary material](#). Thin films of vanadium dioxide (VO<sub>2</sub>) were grown in a hot-wall, horizontal, low-pressure MOCVD system built in-house. The deposition chamber was maintained at 520 °C. Cleaned substrates were mounted on a stainless-steel substrate holder, sloped at  $\sim 15^\circ$  with respect to the horizontal position, placed at the center of the

deposition chamber. Argon was purged as the carrier gas at a flow rate of 100 SCCM. High-purity oxygen was carried through a separate gas line as the reactive gas with a flow rate of 50 SCCM. Depositions of the films were carried out for 15 min. The total pressure in the reactor was maintained at 19.2 Torr by a capacitance manometer. About 0.1 g of the precursor, taken on an aluminum boat, was placed inside the vaporizer at a temperature of 185 °C. The system was evacuated to the base pressure through the purge-line. The furnace, gas lines and the vaporizer were heated to their respective (chosen) temperatures, purging the system with high purity. When all the temperatures were stabilized, the purging with argon gas was stopped and the flow of the carrier gas (argon) and the reactant gas (oxygen) was adjusted to the desired values using Mass Flow Controllers (MFCs). The valve separating the deposition chamber and the vaporizer was then opened initiating film deposition. The total pressure of the system was monitored; the controls were adjusted to maintain a constant pressure. After the deposition time, the carrier gas flow was stopped and the heaters were switched off. Typical deposition conditions are tabulated in Table I.

In this work, a commercially available silicon AFM probe chip was used and a 300 nm thick VO<sub>2</sub> thin film was deposited by CVD technique at 520 °C over it. The AFM probe chip consists of four cantilevers with different dimensions and stiffnesses. Among these, the longest cantilever on the probe was considered to study the thermomechanical actuation of VO<sub>2</sub> thin film. The stiffness of the cantilever was about 0.2 N/m and its resonant frequency was 15 kHz. The corresponding length of the cantilever was 500 μm long, its width was 30 μm and the thickness was 2.7 μm. VO<sub>2</sub> films were deposited directly onto the silicon surface with (100) orientation without any intermediate adhesive/seed layer.

### C. Micromechanical actuation of VO<sub>2</sub> coated microcantilevers

Figure 1(a) shows the experimental set-up used to evaluate the thermomechanical performance of the as-fabricated VO<sub>2</sub> microactuator. For this purpose, a commercially available Peltier thermoelectric heater (TEC1-12706) was used. This heater produced temperatures up to 100 °C for a DC bias of 12 V. Even before the thermal actuation experiments were initiated, the Peltier heater had to be characterized to rule out any non-linearities in its temperature output with respect to applied bias voltage. The heater was connected across a regulated DC power supply and the corresponding temperature rise was measured using a laboratory mercury thermometer. Figure 1(b) shows a linear rise in the heater

temperature with respect to the applied DC bias voltage, while Fig. 1(c) shows the 3D optical profile of a VO<sub>2</sub> coated silicon cantilever.

In this study, thermally excited VO<sub>2</sub> microactuator deflection measurements were performed using an ultra-precision benchtop non-contact 3D optical profilometer (Taylor Hobson-Talysurf CCI). A 3D optical profilometer is basically a measurement interferometer widely used to measure the surface topography of planar samples. Its depth resolution is typically of few tens of nanometer, and hence this type of measurement system allows us to study very small static deflections as well. The Peltier heater was fixed to the XYZ translation stage of the profilometer and the VO<sub>2</sub> microactuator chip was placed over the heater surface. The chip was then heated from room temperature (23 °C) up to 95 °C. The entire chip gets heated by conductive heat transfer from the underlying heater, while some heat may be lost to the environment due to convection. After 5 min, thermal equilibrium is attained and the resulting out-of-plane cantilever deflection was measured using the profilometer. Two sets of measurements have been carried out, i.e., the thermomechanical actuation of an uncoated silicon microcantilever is compared with that of a VO<sub>2</sub> coated microactuator for a temperature range from 23 °C to 95 °C. The results are presented in Sec. III.

## III. RESULTS AND DISCUSSION

### A. Material characterization

The as-deposited VO<sub>2</sub> film was characterized using X-ray diffraction (XRD), scanning electron microscopy (SEM), energy dispersive X-ray spectroscopy (EDX) and Raman spectroscopy. Phase identification of the film was performed by using X-ray diffraction (Cu-K<sub>α</sub> - 1.5418 Å - PANALYTICAL). Structural characterization was also carried out by Raman spectroscopy using a Horiba Jobin Yvon HR-Raman-123 microPL spectrometer with a wavelength of 519 nm. A Carl Zeiss field emission scanning electron microscope (FE-SEM) was employed to probe the microstructure of VO<sub>2</sub> thin films on the cantilever. A DC probe station with a thermal chuck was employed to study the transition characteristics of VO<sub>2</sub> thin films on the cantilever varying the temperature in addition to the temperature variable Raman spectra that probed the transition. Deflection of the cantilever was measured varying the temperature via optical profilometer experiments.

#### 1. X-Ray diffraction (XRD)

X-Ray diffraction studies of the films deposited on Si substrates along with the cantilever under the same deposition conditions at 520 °C were carried out using a XPert Panalytical with Cu-K<sub>α</sub> radiation at a scan rate of 2° per minute. It was observed that the deposited film was crystallized in a M1 phase monoclinic structure as shown in Fig. 2. The peak positions in this pattern were consistent with the M1 phase (monoclinic structure). The peaks matched with JCPDS card no. 82-0661. The major peaks were at 27.53° (011) and 36.72° (-211) revealing phase purity and polycrystalline nature of the films. Also, peaks corresponding to

TABLE I. Deposition parameters for VO<sub>2</sub> thin films.

Parameters	Value
Furnace temperature	520 °C
Deposition time	15 min
Oxygen flow rate	50 SCCM
Argon flow rate	100 SCCM
Vaporizer temperature	185 °C
Pressure	19.2 Torr

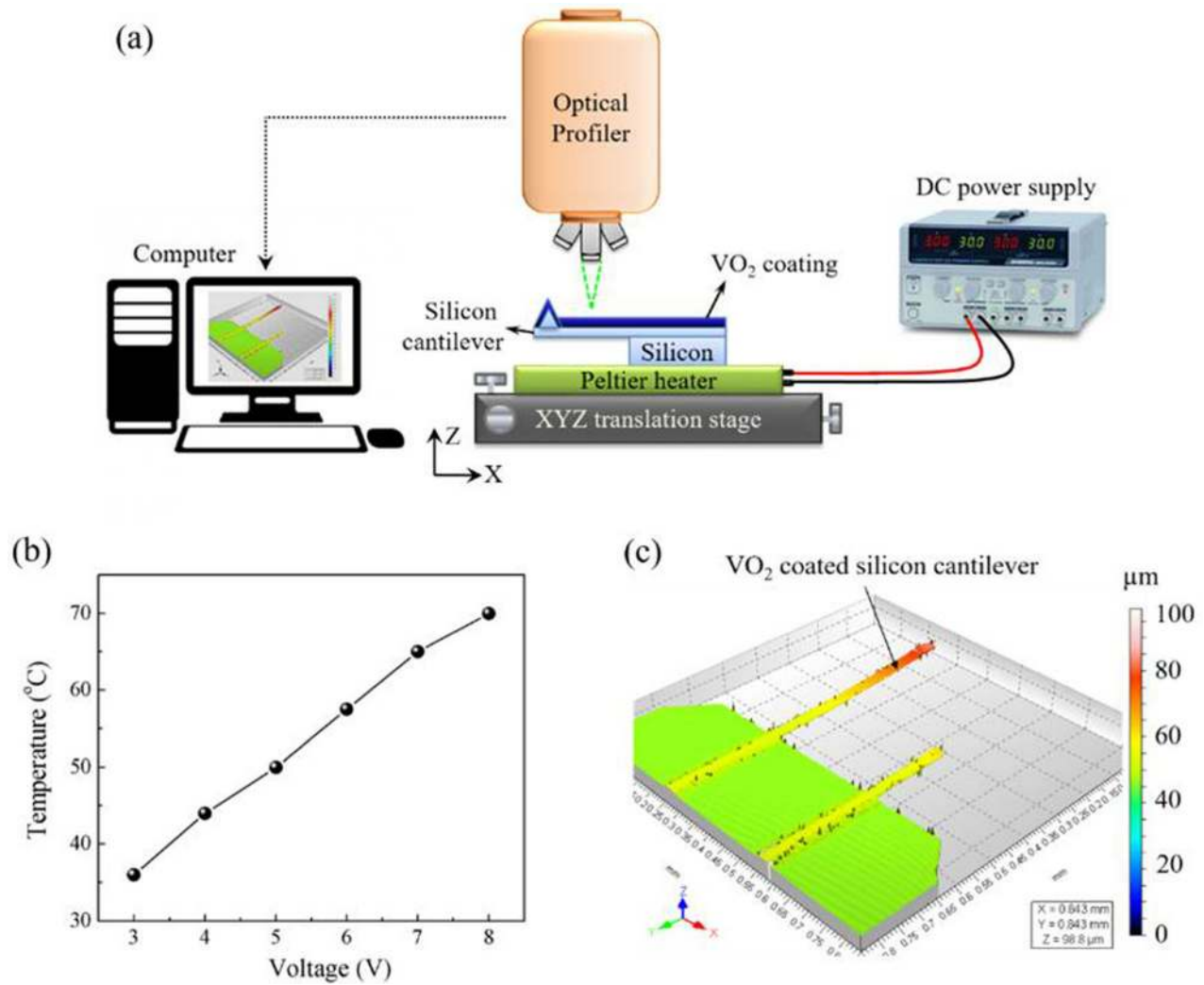


FIG. 1. (a) Schematic showing the experimental set-up used to study the thermomechanical actuation in a VO<sub>2</sub> coated silicon microcantilever. (b) Linear behavior of the Peltier heater. (c) 3D optical profile of the VO<sub>2</sub> coated silicon cantilever when heated to 65 °C.

other impurity phases did not appear in the pattern within the resolution limit, thereby confirming the single-phase nature of the thin films. Though the confirmation of monoclinic phase characterization of thin films by powder XRD has its

limitations, Raman studies provided further confirmation of the M1 phase.

## 2. Raman spectroscopy

Room temperature and temperature variable Raman spectra were acquired for VO<sub>2</sub> films deposited on silicon cantilevers. Figure 3(a) shows the optical images of the cantilever surface on which Raman spectra were recorded. They were identified with the M1 phase of monoclinic VO<sub>2</sub> as can be seen in Fig. 3(b). A temperature variable Raman spectrum is shown in Fig. 3(c) and the peak intensity of 192 cm<sup>-1</sup> with respect to temperature is plotted in Fig. 3(d). The peaks were located at the wave numbers: 139, 192, 223, 261, 307, 336, 390, 440, 499, 612 and 823 cm<sup>-1</sup>. There is a polymorph of VO<sub>2</sub> that exists in M2, T, and R phases. Raman spectra become quintessential to differentiate these polymorphs. This difference between M1 and M2 phases occurs in the shifting of 607 and 189 cm<sup>-1</sup> energies to higher values, in addition to a decrease in the 444 cm<sup>-1</sup> mode and the splitting of 225 cm<sup>-1</sup> in the M1 mode.<sup>30</sup> Density functional theory calculations suggest that the two low-frequency phonons correspond to the V-V lattice motion<sup>31</sup> and all other peaks are

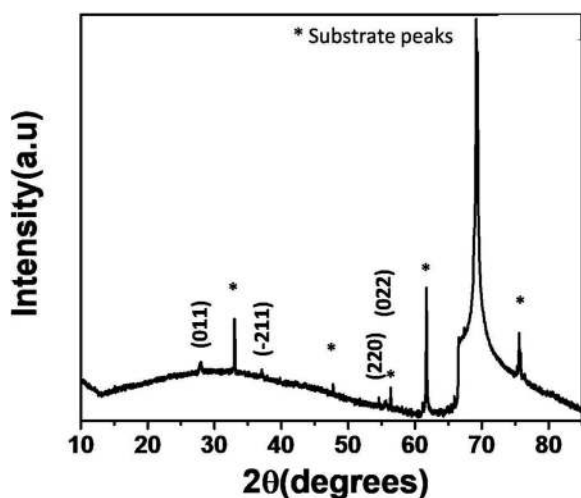


FIG. 2. X-Ray diffraction of VO<sub>2</sub> thin films deposited on a silicon substrate.

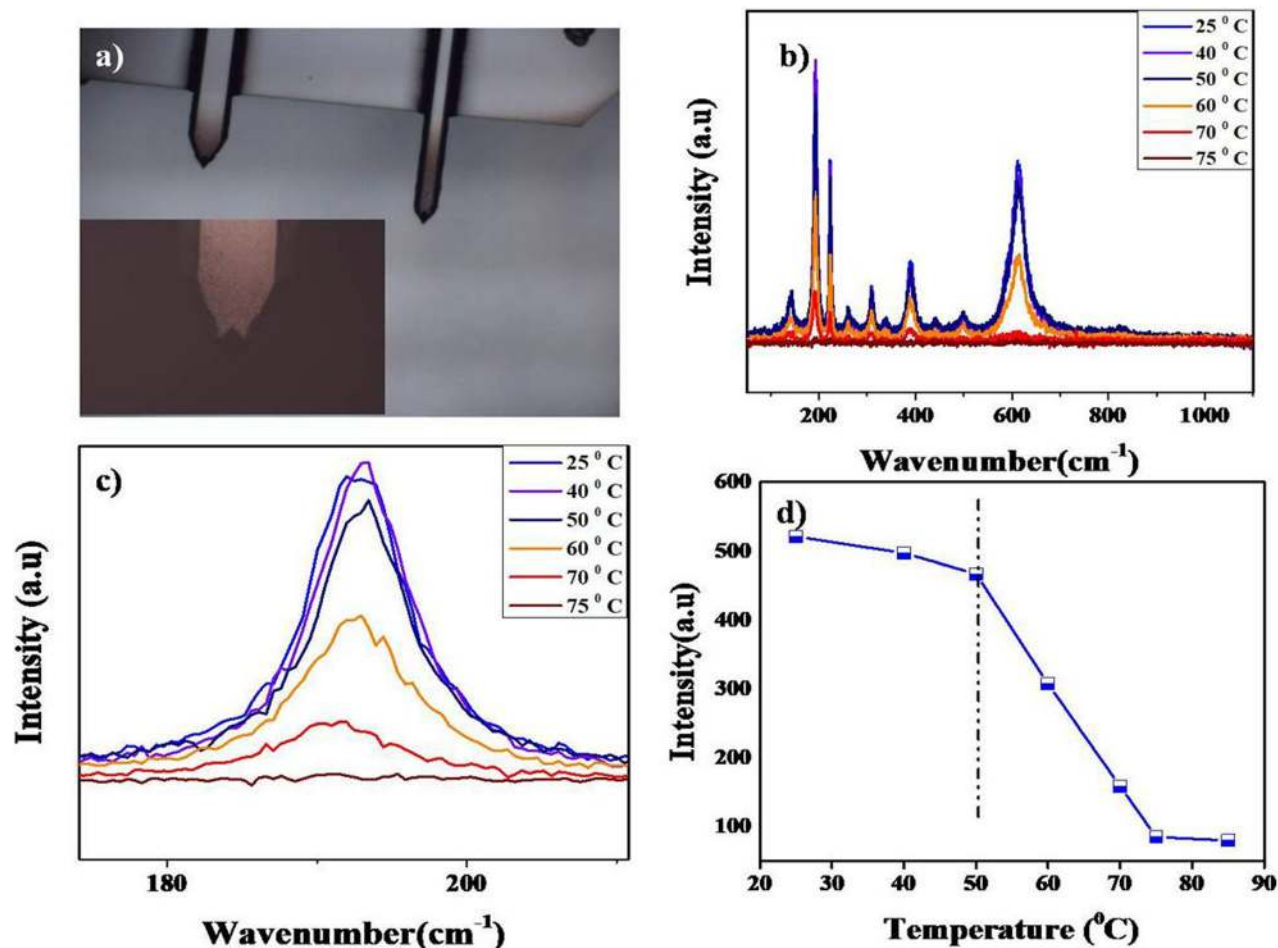


FIG. 3. (a) Optical images of the VO<sub>2</sub> coated cantilevers in which Raman spectra were recorded. (b) Temperature variable Raman spectra showing the peaks corresponding to the M1 monoclinic phase transitioning during the phase transition. (c) Temperature variable spectra showing the variation in the intensity of the 192 cm<sup>-1</sup> peaks with respect to temperature. (d) Transition temperature calculated from intensity variation of the 192 cm<sup>-1</sup> peaks.

distinguished to be related to V-O bonding.<sup>32</sup> In the present work, eleven peaks were identified and tabulated as phonon modes of monoclinic M1 in Table II. Eight A<sub>g</sub> modes and two B<sub>g</sub> modes were identified along with one E<sub>g</sub> mode. These results are compared with previous studies.<sup>30–32</sup> Raman spectra of the VO<sub>2</sub> samples before and after the transition are plotted in Fig. 3(b). Almost all the Raman modes were available at room temperature and VO<sub>2</sub> was present in the monoclinic M1 phase. Temperature was varied and the spectrum was recorded at an interval of 10 °C. Reduction in the peak intensity and change in the profile highlighted the transition of VO<sub>2</sub>. After the transition, the peak intensity reduced, suggesting that it has transitioned to the tetragonal crystal structure as seen in several reports. The peaks disappeared after the transition confirming the tetragonal nature of VO<sub>2</sub>. From the data on peak intensity, one can also quantify the hysteresis present in the sample with both heating and cooling data.

### 3. Scanning electron microscopy (SEM) and energy dispersive X-ray spectroscopy (EDX)

The surface morphology of as-deposited VO<sub>2</sub> films on the silicon substrate was studied using scanning electron microscopy. Figures 4(a)–4(c) show the SEM image of a

continuous VO<sub>2</sub> film formed by granular nanoparticles on a silicon cantilever. Figure 4(c) indicates spherical nanoparticles whose grain boundaries overlap to produce a continuous dense film. The films deposited by CVD technique results in large crystallites on a silicon surface with an average grain size in the range 200–250 nm. The elemental composition of the deposited VO<sub>2</sub> film was evaluated using EDX analysis which indicates the presence of oxygen and vanadium. There are two major peaks corresponding to the silicon substrate and the underlying carbon adhesive tape. Also, a small peak corresponding to aluminum is seen due to the reflective coating underside the silicon cantilever.

### B. Electrical switching in VO<sub>2</sub> film

The electrical properties of the VO<sub>2</sub> thin film was characterized along in-plane geometry using two-probe measurement technique. For this purpose, a DC probe station (PM5 with thermal chuck, Agilent Device Analyzer B1500A) was used. All electrical measurements were directly carried out on VO<sub>2</sub> coated over a silicon AFM probe chip under ambient conditions. To the best of our knowledge, this approach of direct electrical characterization of VO<sub>2</sub> cantilever thin films has not been carried out before. This approach may be accurate and reliable in the comprehension of correlated

TABLE II. Comparison of Raman spectral peaks reported in the literature with those obtained in this work for a 300 nm VO<sub>2</sub> thin film.

$\lambda$ (cm <sup>-1</sup> ) <sup>a</sup>	$\lambda$ (cm <sup>-1</sup> ) <sup>b</sup>	$\lambda$ (cm <sup>-1</sup> ) <sup>c</sup>	$\lambda$ (cm <sup>-1</sup> ) <sup>d</sup>
149	...	143	147
199	191	192	194
225	222	223	222
259	262	262	262
265	...	...	...
313	305	306	305
339	337	387	337
392	390	...	390
395	...	...	...
444	443	495	443
453	...	...	495
489	497	...	...
503	535	...	...
595	...	...	...
618	613	610	616
1670	...	...	...
830	...	...	823

<sup>a</sup>Wavenumber corresponding to RF sputtering of the epitaxial VO<sub>2</sub> thin film as discussed by Jones *et al.* in Ref. 30.

<sup>b</sup>Wavenumber corresponding to electrodeposition of the epitaxial VO<sub>2</sub> thin film as discussed by Wu *et al.* in Ref. 31.

<sup>c</sup>Wavenumber corresponding to hydrothermal synthesis of VO<sub>2</sub> as discussed by Wu *et al.* in Ref. 32.

<sup>d</sup>Wavenumber corresponding to chemical vapor deposition of the VO<sub>2</sub> thin film as discussed in the present work.

electrical and thermomechanical switching phenomena in VO<sub>2</sub> coated MEMSs. Temperature was varied from room temperature (25 °C) up to 110 °C and the corresponding current–voltage (I–V) characteristics of the VO<sub>2</sub> thin film was recorded. These measurements were tested for reproducibility by repeatedly performing the experiment thrice. Figure 5(a) shows the temperature dependence of the normalized resistance  $R(T)/R(25\text{ }^\circ\text{C})$ . Examining the resistance versus temperature (R–T plot) of the thin films, an abrupt first order transition about three orders of magnitude is observed. The reciprocal slope of linear I–V scans at each temperature determines the resistance of the film at the corresponding temperature. Prior to this, contact between the VO<sub>2</sub> film and the probes was found to be linear and ohmic. The semiconductor-metal transition temperature ( $T_{\text{SMT}}$ ) is defined as the peak in the  $d(\log(R))/dT$  versus T (derivative curve of R–T) plot in Fig. 5(b) for heating and cooling. The reported VO<sub>2</sub> thin films showed that the transition temperature was 74 °C. Hysteresis measured by the electrical resistance between the heating and cooling cycles is minimal, but the width of the transition was measured to be around 15 °C for heating and 20 °C for the cooling cycle. The electrical response is slower than the optical response of VO<sub>2</sub> and it has been reported earlier in the literature.<sup>33</sup>

### C. Micromechanical actuation in VO<sub>2</sub> coated microcantilever using a 3D-optical profiler

The silicon AFM chip used in this actuation study consists of 4 cantilevers with varying dimensions and stiffnesses. Thermomechanical actuation measurements were

carried out on the longest cantilever on the chip ( $L = 500\ \mu\text{m}$ ) as indicated in Fig. 4(a). A VO<sub>2</sub> microactuator was placed on a Peltier heater which provides uniform temperature distribution. Upon heating from 23 °C to 95 °C, the actuator showed very large, reversible structural deformation. The thermomechanical actuation in a VO<sub>2</sub> coated silicon microcantilever was measured using a non-contact 3D optical profilometer. Figures 6(a)–6(d) illustrate the deflection profile of a bare (uncoated) silicon cantilever and a VO<sub>2</sub> coated silicon cantilever. Both the cantilevers were placed over a Peltier heater and heated from room temperature (23 °C) up to 95 °C. All the experiments reported in this paper were carried out under ambient conditions. At room temperature, the bare cantilevers obtained commercially are seen to have a straight profile without any residual stress or curvature [Fig. 6(a)]. However, upon further heating, the cantilever shows a slight deflection of 0.9  $\mu\text{m}$  at 50 °C as seen in Fig. 6(c). This may be due to the presence of 30 nm thin film of aluminum on one side of the silicon cantilever. Figure 6(b) indicates the 3D profile of VO<sub>2</sub> coated cantilevers at room temperature exhibiting an inherent curvature which is attributed to the residual stress induced during the deposition of the VO<sub>2</sub> thin film on the silicon surface.<sup>34</sup> Upon further heating, the VO<sub>2</sub> coated cantilever showed a large tip deflection of about 14  $\mu\text{m}$  at 50 °C [see Fig. 6(d)]. The as-deposited VO<sub>2</sub> film undergoes first order phase transition from the monoclinic phase (011)<sub>M1</sub> at room temperature to a tetragonal phase (110)<sub>R</sub> at 50 °C. At this temperature, the volume per unit cell of the VO<sub>2</sub> crystallite along the  $c_R$ -axis decreases resulting in the contraction/compression of the VO<sub>2</sub> film.<sup>35</sup> Hence, the VO<sub>2</sub> coated cantilever undergoes an upward deflection as seen in Fig. 6(e). The heating and cooling cycles produce a concurrent phase change in the highly oriented VO<sub>2</sub> films, and thus the induced stress in the VO<sub>2</sub> film contributes to the deflection of VO<sub>2</sub>/Si structure. In comparison, the thermal stress in the bare silicon cantilever only showed a maximum tip deflection of 0.9  $\mu\text{m}$  at 50 °C, which is less than 6.4% with respect to VO<sub>2</sub> coated cantilever. Hence, the effects of thermal stress can be neglected for further thermomechanical analysis.

1D static deflection profile of the VO<sub>2</sub> microactuator is indicated in Fig. 7(a). In this case, the first order phase transition at 50 °C produces a maximum tip deflection of 14  $\mu\text{m}$  relative to its position at room temperature. On further heating up to 95 °C, there is no significant change in the deflection. The same can be observed while cooling the microactuator. This phenomenon of reversible, bi-stable micromechanical switching of VO<sub>2</sub> coated MEMS structures makes it suitable for applications in memory devices.<sup>22</sup> Figure 7(a) indicates an upward bending of the VO<sub>2</sub> coated microcantilever owing to the compressive stresses generated within the VO<sub>2</sub> film at its transition temperature (50 °C). It may be worth noting that in each sample, the temperature at which SMT occurs is different for electrical switching (74 °C) and mechanical deformation (50 °C).<sup>36</sup> For thermal actuation and scalability issues, CVD will suffice.

Figure 7(b) shows the actuation response of the reported VO<sub>2</sub> microactuator. The plot indicates the tip deflection of the cantilever at various temperatures for both VO<sub>2</sub> coated cantilevers and bare uncoated cantilevers. From these results,

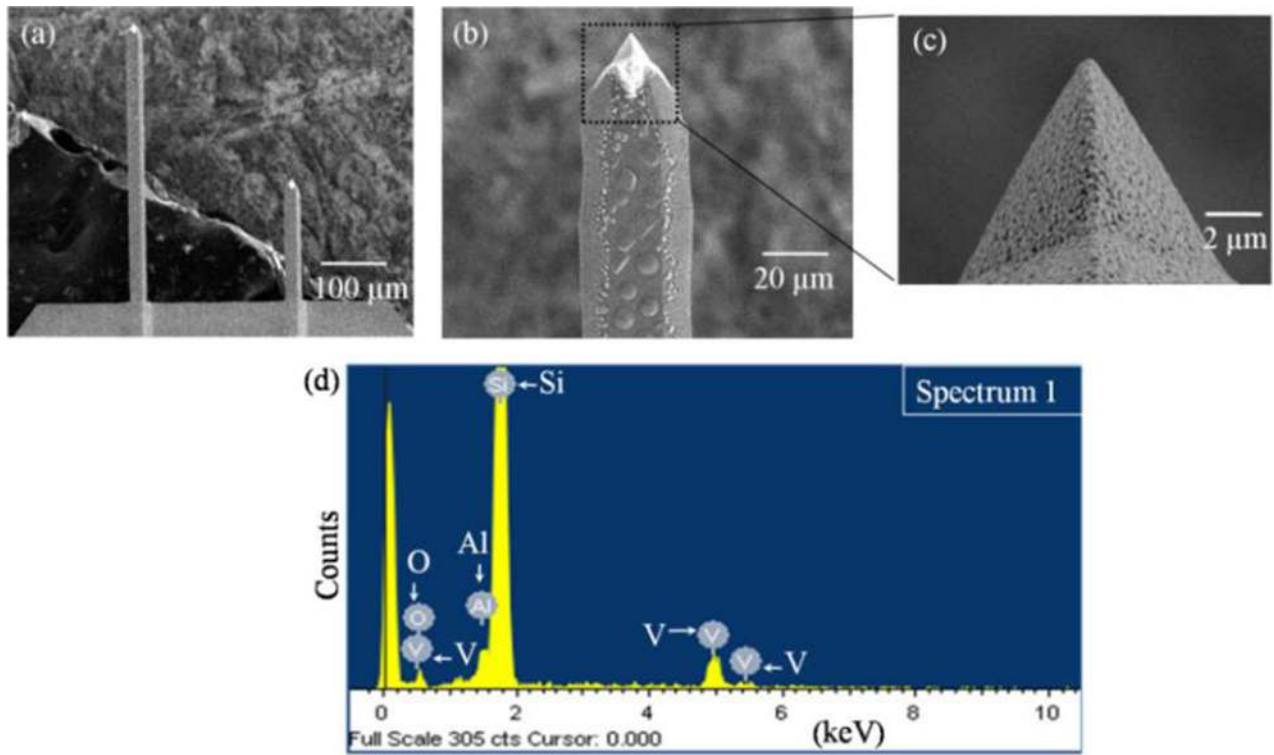


FIG. 4. (a) SEM image of the silicon cantilever showing the longest cantilever with a length of  $500\ \mu\text{m}$ . (b) SEM image showing  $\text{VO}_2$  coating on the Si cantilever. (c) SEM image showing uniform deposition of  $\text{VO}_2$  at the cantilever tip. (d) EDX spectra showing the elemental constituents of the deposited  $\text{VO}_2$  film on the silicon cantilever.

it may be observed that the uncoated cantilever showed a small deflection of about  $1.26\ \mu\text{m}$  for a maximum temperature of  $95\ ^\circ\text{C}$ . These values serve as base/reference deflection. Furthermore,  $\text{VO}_2$  coated cantilevers produced a large, reversible tip deflection of  $14\ \mu\text{m}$  at  $50\ ^\circ\text{C}$ . This may be attributed to the superior quality of the  $\text{VO}_2$  film deposited using MOCVD technique as well as the unique deflection measurement technique employed. From Fig. 7(b), it may be observed that the cantilever deflection changes with respect to the applied temperature and the slope of deflection is the steepest at transition temperature ( $50\ ^\circ\text{C}$ ). These results show reversible cantilever deflection for heating and cooling cycles with low hysteresis.

#### IV. CONCLUSION

This paper presents micromechanical actuation of a  $\text{VO}_2$  coated silicon microcantilever using the phenomenon of thermally excited phase transition. CVD technique was employed to deposit a  $300\ \text{nm}$   $\text{VO}_2$  film over a silicon microcantilever at  $520\ ^\circ\text{C}$ . The major peaks at  $27.53^\circ$  (011) and  $36.72^\circ$  ( $-211$ ) indicate the single-phase, polycrystalline nature of  $\text{VO}_2$  film. Raman spectra obtained for the as-deposited  $\text{VO}_2$  films indicated the presence of pure monoclinic M1 phase. Temperature variable Raman spectra verified the phase transition. Scanning electron microscopy shows continuous  $\text{VO}_2$  film formed by granular nanoparticles on silicon cantilever.  $\text{VO}_2$  films

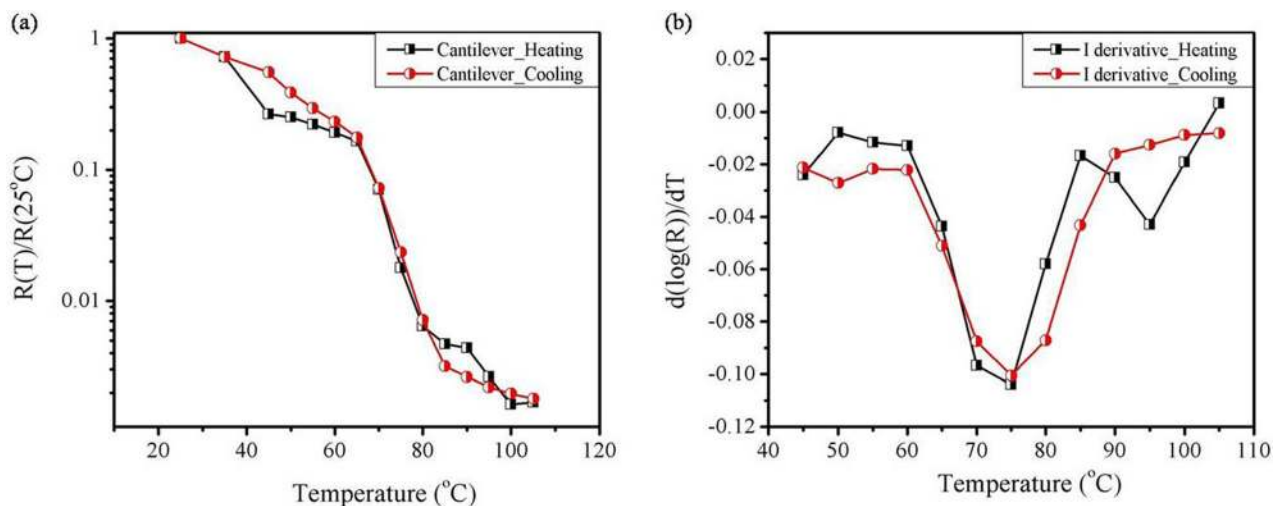


FIG. 5. (a) Electrical characteristics of the  $\text{VO}_2$  thin film deposited on the cantilever. (b)  $dR/dT$ —the first derivative curve to understand the transition characteristics.

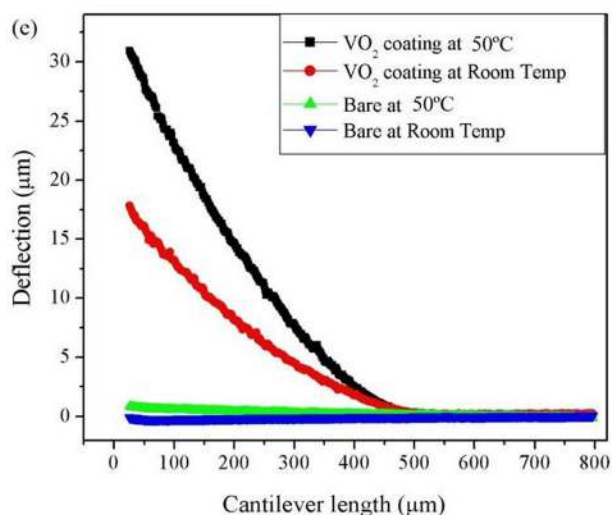
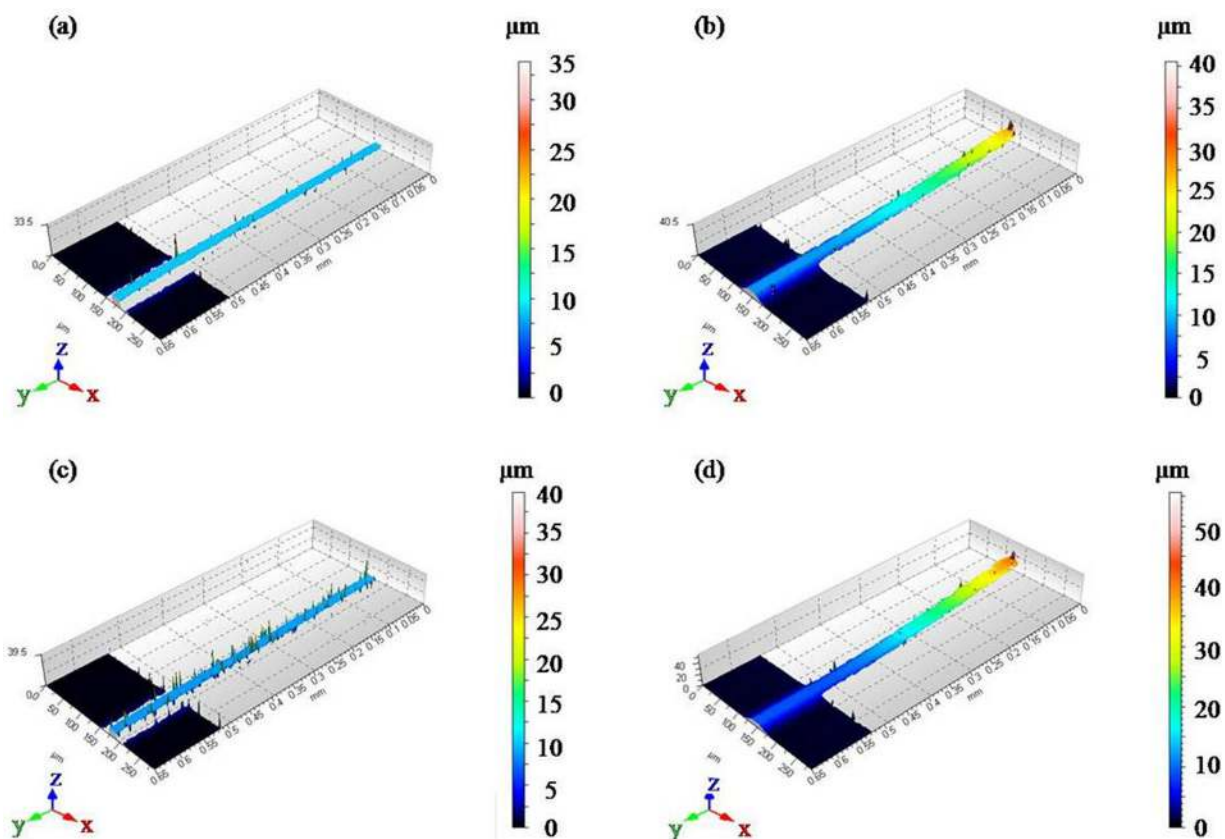


FIG. 6. Deflection profiles of a thermally actuated silicon microcantilever using an optical profiler (a) and (c) 3D deflection profile of bare silicon cantilevers at room temperature and at 50 °C, respectively. (b) and (d) 3D deflection profile of the VO<sub>2</sub> coated silicon cantilever at room temperature and at 50 °C, respectively. (e) 1D representation of a bare cantilever and VO<sub>2</sub> coated cantilevers showing the inherent curvature of the VO<sub>2</sub> coated silicon cantilever at room temperature and its relative tip deflection at 50 °C.

deposited by MOCVD technique result in large crystallites on the silicon surface with an average grain size in the range 200–250 nm. The electrical characterization of the VO<sub>2</sub> film produced semiconductor-to-metal transition (SMT) at 74 °C and the change in the electrical resistance of the VO<sub>2</sub> film was measured to be about three orders of magnitude. Consequently, the VO<sub>2</sub> film undergoes structural phase transition from the monoclinic phase (011)<sub>M1</sub> at room temperature to a tetragonal phase (110)<sub>R</sub> at 50 °C. This generates a compressive stress within the VO<sub>2</sub> film resulting in large,

reversible cantilever deflection, which was measured with a non-contact 3D optical profilometer which does not require any vacuum conditions or expensive equipment such as TEM or SEM. Also, the issues of laser spot alignment over a small cantilever surface can be overcome. A maximum tip deflection of 14 μm was measured at 50 °C during the first order phase transition in VO<sub>2</sub> coated cantilever. For micromechanical actuation, the transition temperature was found to be about 50 °C which is much lesser than the electrical transition temperature (74 °C). Several heating and cooling cycles revealed

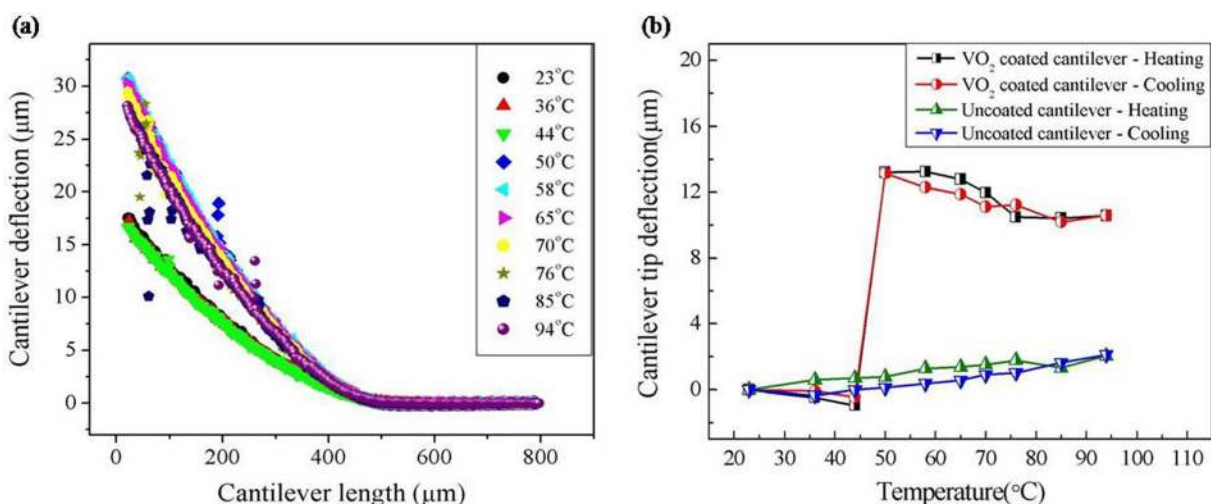


FIG. 7. (a) 1D deflection profile of the  $\text{VO}_2$  coated cantilever showing mechanical switching at  $50^\circ\text{C}$ . (b) Maximum cantilever tip deflection for uncoated and  $\text{VO}_2$  coated silicon microcantilevers at various temperatures from room temperature up to  $94^\circ\text{C}$ .

good repeatability and negligible hysteresis. From these experimental results, it may be concluded that the uncoated silicon microcantilever only showed a small deflection of about  $0.9\ \mu\text{m}$  at the transition temperature. Therefore, the effect of thermal stress arising in the cantilever was estimated to be as small as 6.4%, and hence can be ignored.

## SUPPLEMENTARY MATERIAL

See [supplementary material](#) for the synthesis and characterization details related to precursors used in the CVD process and it also briefs about the deposition of  $\text{VO}_2$  thin films.

## ACKNOWLEDGMENTS

The authors would like to thank Micro Nano Characterization Facility (MNCf) at Centre for Nano Science and Engineering (CeNSE), Indian Institute of Science, Bengaluru, for providing the characterization facilities. B.R. would like to thank Mr. Jude Inyalot Tadeo for his help in temperature variable Raman measurements.

- <sup>1</sup>J. Singh, K. Rajanna, B. Umapathi, M. M. Nayak, and K. Nagachenchaiah, *IEEE Sens.* 1129–1132 (2011).
- <sup>2</sup>Y. Fukuta, Y.-A. Chapuis, Y. Mita, and H. Fujita, *J. Microelectromech. Syst.* **15**, 912 (2006).
- <sup>3</sup>M. Boudaoud, Y. Haddab, and Y. Le Gorrec, in *Proceedings of the IEEE/RSJ International Conference on Intelligent Robots and Systems*, Taipei, Taiwan, 18–22 October 2010 (IEEE, 2010).
- <sup>4</sup>L. Maignon, G. J. Laurent, N. Le Fort-Piat, and Y.-A. Chapuis, *J. Intell. Rob. Syst.* **59**, 145 (2010).
- <sup>5</sup>M. Patrascu, J. Gonzalo-Ruiz, M. Goedbloed, M. Crego-Calama, and S. H. Brongersma, *Proc. Eng.* **25**, 1181 (2011).
- <sup>6</sup>S. Büttgenbach, S. Bütetfisch, M. Leester-Schädel, and A. Wogersien, *Microsyst. Technol.* **7**, 165 (2001).
- <sup>7</sup>J. Yang and H. J. Xiang, *Smart Mater. Struct.* **16**, 784 (2007).
- <sup>8</sup>L. U. Haiwei and Z. H. U. Jianguo, “A comparative study of microactuators driven by electric and magnetic principles,” in *Australasian Universities Power Engineering Conference (AUPEC 2004)*, Brisbane, Australia, 26–29 September 2004.
- <sup>9</sup>J. S. Ko, M. L. Lee, D.-S. Lee, C. A. Choiand, and Y. T. Kim, *Appl. Phys. Lett.* **81**, 547 (2002).
- <sup>10</sup>L. R. Viannie, S. Joshi, G. R. Jayanth, V. Radhakrishna, and K. Rajanna, in *Proceedings of the IEEE Sensors*, Taipei (2012).

- <sup>11</sup>A. Baracu, R. Voicu, R. Müller, A. Avram, M. Pustan, R. Chiorean, C. Birleanu, and C. Dulescu, *AIP Conf. Proc.* **1646**, 25 (2015).
- <sup>12</sup>L. R. Viannie, G. R. Jayanth, V. Radhakrishna, and K. Rajanna, *J. Microelectromech. Syst.* **25**, 125 (2016).
- <sup>13</sup>E. Merced, D. Torres, X. Tan, and N. Sepulveda, *J. Micromech. Syst.* **25**(4), 543 (2016).
- <sup>14</sup>N. R. Mlyuka, G. A. Niklasson, and C. G. Granqvist, *Appl. Phys. Lett.* **95**, 171909 (2009).
- <sup>15</sup>S. Kumar, F. Maury, and N. Bahlawane, *Sci. Rep.* **6**, 37699 (2016).
- <sup>16</sup>Y. Ji, Y. Zhang, M. Gao, Z. Yuan, Y. Xia, C. Jin, B. Tao, C. Chen, Q. Jia, and Y. Lin, *Sci. Rep.* **4**, 4854 (2014).
- <sup>17</sup>J. Cao, W. Fan, Q. Zhou, E. Sheu, A. Liu, C. Barrett, and J. Wu, *J. Appl. Phys.* **108**, 083538 (2010).
- <sup>18</sup>C. Ko, Z. Yang, and S. Ramanathan, *Annu. Rev. Mater. Res.* **41**, 337 (2011).
- <sup>19</sup>T. Wang, D. Torres, F. E. Fernandez, A. J. Green, C. Wang, and N. Sepulveda, *ACS Nano* **9**, 4371 (2015).
- <sup>20</sup>M. A. Kats, D. Sharma, J. Lin, P. Genevet, R. Blanchard, Z. Yang, M. Mumtaz Qazilbash, D. N. Basov, S. Ramanathan, and F. Capasso, *Appl. Phys. Lett.* **101**, 221101 (2012).
- <sup>21</sup>A. Tselev, I. A. Luk'yanchuk, I. N. Ivanov, J. D. Budai, J. Z. Tischler, E. Strelcov, A. Kolmakov, and S. V. Kalinin, *Nano Lett.* **10**, 4409 (2010).
- <sup>22</sup>R. Cabrera, E. Merced, and N. Sepúlveda, *J. Micromech. Syst.* **23**, 243 (2014).
- <sup>23</sup>H. Guo, K. Wang, Y. Deng, Y. Oh, S. A. Syed Asif, O. L. Warren, Z. W. Shan, J. Wu, and A. M. Minor, *Appl. Phys. Lett.* **102**, 231909 (2013).
- <sup>24</sup>R. Cabrera, E. Merced, and N. Sepúlveda, *Phys. Status Solidi A* **210**, 1704 (2013).
- <sup>25</sup>B. Viswanath and S. Ramanathan, *Nanoscale* **5**, 7484 (2013).
- <sup>26</sup>R. Cabrera, E. Merced, N. Dávila, F. E. Fernández, and N. Sepúlveda, *Microelectron. Eng.* **88**, 3231 (2011).
- <sup>27</sup>E. Merced, N. Davila, D. Torres, R. Cabrera, F. E. Fernandez, and N. Sepulveda, *Smart Mater. Struct.* **21**, 105009 (2012).
- <sup>28</sup>U. Ail, *Thin Film Semiconducting Metal Oxides by Nebulized Spray Pyrolysis and MOCVD, for Gas-Sensing Applications (Materials Research Centre, Indian Institute of Science, 2008)*.
- <sup>29</sup>M. B. Sahana, *Metal Organic Chemical Vapour Deposition of Thin Films of Vanadium Oxides: Microstructure and Properties (Materials Research Centre, Indian Institute of Science, 2003)*.
- <sup>30</sup>A. C. Jones, S. Berweger, J. Wei, D. Cobden, and M. B. Raschke, *Nano Lett.* **10**, 1574 (2010).
- <sup>31</sup>J. M. Wu and L. B. Liou, *J. Mater. Chem.* **21**, 5499 (2011).
- <sup>32</sup>Y. F. Wu, L. L. Fan, S. M. Chen, S. Chen, C. W. Zou, and Z. Y. Wu, *AIP Adv.* **3**, 042132 (2013).
- <sup>33</sup>R. Bharathi, R. Naorem, and A. M. Umarji, *J. Phys. D: Appl. Phys.* **48**, 305103 (2015).
- <sup>34</sup>B. Viswanath, C. Ko, Z. Yang, and S. Ramanathan, *J. Appl. Phys.* **109**, 063512 (2011).
- <sup>35</sup>J. Bowen and D. Cheneler, *Nanoscale* **8**, 4245 (2016).
- <sup>36</sup>D. Singh and B. Viswanath, *Scr. Mater.* **141**, 24 (2017).